Applied Surface Science 688 (2025) 162430

Contents lists available at ScienceDirect

Applied Surface Science

journal homepage: www.elsevier.com/locate/apsusc

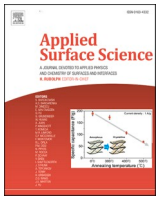

Full Length Article

Structural characterisation and dynamic modelling of pegylated graphene oxide with Ag and Cu nanocluster

Miriam Roldán-Matilla [a], Patrick Irigo [b], María Luisa Rojas-Cervantes [c], Mariana P. Arce [d], Javier Pérez-Piñeiro [d], María Fuencisla Gilsanz [d], Isabel Lado-Touriño [e,*], Arisbel Cerpa-Naranjo [e,*], Guogang Ren [b,**]

[a] Professional Formation Centre. European University of Madrid, Villaviciosa de Odón, 28670 Madrid, Spain
[b] Technology Research Institute, University of Hertfordshire, Hatfield, Herts AL10 9AB, UK
[c] Department of Inorganic and Technical Chemistry, Universidad Nacional de Educación a Distancia (UNED), Urbanización Monterrozas, Las Rozas 28232, Madrid, Spain
[d] Department of Sciences and Aerospatial, School of Architecture, Engineering, Science and Computing. European University, Villaviciosa de Odón, 28670 Madrid, Spain
[e] Department of Engineering. School of Architecture, Engineering, Science and Computing. European University, Villaviciosa de Odón, 28670 Madrid, Spain

ARTICLE INFO

Keywords:
Graphene
Graphene oxide
PEGylation
Nanoparticles
Clusters
Molecular dynamics
Exfoliation
Stability

ABSTRACT

Graphene (G) and graphene oxide (GO) are increasingly employed in energy, materials, and healthcare sectors. Silver (Ag) and copper (Cu) nanomaterials, including their nanoclusters, are crucial for advanced antimicrobial therapies and improving the performance of materials in energy and biomedical applications. However, achieving uniform dispersion and stability in both hydrophobic and hydrophilic environments remain a challenge. This study addresses these challenges by synthesizing and characterizing PEGylated GO_{30} functionalised with Ag and Cu nanoclusters through amide bond formation. Using TEM, SEM, UV–Visible spectroscopy, FTIR, Raman spectroscopy, TGA, and molecular dynamics (MD) simulations, we identified optimal strategies and mechanism for stabilising these nanoclusters as well as the nanostructures. The oxidation and subsequent PEGylation of graphene significantly enhance the interaction energy of Ag nanoclusters by 239.47 kcal/mol and Cu nanoclusters by 259.98 kcal/mol. This functionalisation (GO-PEG-NH_2) also substantially reduces nanocluster mobility on the graphene-based surface, with mean squared displacement (MSD) values of 20–30 $Å^2$ at 500 ps, compared to 150–175 $Å^2$ for non-functionalised graphene clusters. SEM and TEM analyses show that PEGylation promotes nanoparticle dispersion and reduces aggregation on GO_{30} sheets, achieving a more consistent size distribution of 10–20 nm. U-Visible spectroscopy reveals that PEGylated Ag nanoparticles exhibit a stable plasmonic response between 400–450 nm, while the broadening of decomposition peaks indicates improved thermal stability and uniform heat distribution. Overall, PEGylation markedly enhances the stability, dispersion, and functionality of metal nanoclusters on graphene-based materials, underscoring their potential for drug delivery, antimicrobial technologies, and energy storage, while laying a strong foundation for future research in functional nanomaterials.

1. Introduction

Graphene has attracted significant attention in material science, energy and biomedical due to its exceptional properties, including its single layer of carbon atoms arranged in a hexagonal lattice with sp2 hybridized bonds. Graphene is known for its outstanding electrical conductivity [1], mechanical strength [2], and thermal stability [3]. Meanwhile, graphene oxide (GO), a derivative of graphene produced via oxidative exfoliation of graphene, offers additional advantages [4,5]. GO's hydroxyl (–OH), epoxy, and carboxyl (–COOH) groups can enhance its dispersibility in both hydrophobic and hydrophilic solvents and enable their easy surface modification [6,7]. These functionalities

* Corresponding autors at: c: Tajo s/n. Villaviciosa de Odón, 28670 Madrid, Spain.
** Corresponding autor at: University of Hertfordshire, Hatfield, Herts AL10 9AB, UK.
E-mail addresses: miriam.roldan@universidadeuropea.es (M. Roldán-Matilla), p.irigo2@herts.ac.uk (P. Irigo), mrojas@ccia.uned.es (M.L. Rojas-Cervantes), mariana.arce@universidadeuropea.es (M.P. Arce), javier.perez4@universidadeuropea.es (J. Pérez-Piñeiro), mariafuencisla.gilsanz@universidadeuropea.es (M.F. Gilsanz), misabel.lado@universidadeuropea.es (I. Lado-Touriño), arisbel.cerpa@universidadeuropea.es (A. Cerpa-Naranjo), g.g.ren@herts.ac.uk (G. Ren).

https://doi.org/10.1016/j.apsusc.2025.162430
Received 1 October 2024; Received in revised form 23 December 2024; Accepted 14 January 2025
Available online 19 January 2025

allow GO to form covalent bonds with various functional groups [8], polymers [9], and drugs [10], making it ideal for applications which requiring advanced material integration and versatility [11,12].

In particular. the large specific surface area of GO makes it ideal for loading a range of therapeutic agents, including drugs, functional nanoparticles and nanoclusters [13,14]. Sanchez et al. explored the interactions between graphene-based nanomaterials and biological systems and underscored the importance of detailed material characterisation to address potential cytotoxicity and optimise their applications in drug delivery and biosensing [15]. While GO provides enhanced dispersibility and functionalisation compared to graphene, its lower electronic conductivity and potential stability issues may limit its effectiveness in antimicrobial treatments and drug delivery [16,17]. Conjugating GO with PEG—a technique known as PEGylation— significantly enhances its synergistic properties, [18,19,20]. With non-aminated PEG, the carboxyl groups on the GO surface undergo esterification by reacting with the hydroxyl groups of PEG chains [21]. In contrast, aminated PEG (PEG-NH_2), which features amino groups at the chain ends, forms amide bonds with these carboxyl groups through amidation under appropriate activation conditions [22]. The PEGylation process improves its interaction with metal nanoparticles, resulting in better dispersion and nano-stability [14]. Specifically, PEG-NH_2 offers distinct benefits, including stronger and more stable covalent bonds, greater chemical and thermal stability, and increased versatility for further functionalisation. These properties enhance material performance, positioning PEG-NH_2 as an ideal choice for applications such as drug delivery and catalysis, where stability and adaptability are critical [23,24,25,26]. For covalent bonding to occur, drugs, metallic nanoparticles, or biomolecules must be functionalised and chemically activated to react with the amino groups of PEG-NH_2. Covalent bonds provide superior stability and durability, making them particularly advantageous for applications requiring robustness and resistance to environmental changes, such as catalysis or the long-term transport and controlled release of drugs [22 27,28]. In the absence of chemical activation, non-covalent interactions like electrostatic forces and Van der Waals interactions predominate [26]. At acidic pH, the amino groups are protonated, acquiring a positive charge that enhances electrostatic interactions with negatively charged nanoparticles or biomolecules, thereby increasing retention and stability on the functionalised surface. Conversely, under neutral or slightly basic pH, the amino groups of PEG-NH_2 remain uncharged, reducing the strength of electrostatic interactions and leading to weaker interactions dominated by Van der Waals forces. Non-covalent interactions, being more sensitive to external stimuli like pH and temperature, offer dynamic and reversible behaviour, which is desirable for applications such as sensing, bio-detection, or antimicrobial activity, where adaptability is key [26]. Additionally, the uncharged state of the amino groups can promote coordination interactions with metal surfaces, further broadening the material's versatility [27,28,29]. Furthermore, PEG-NH_2 functionalisation provides significant advantages in drug delivery systems, particularly for hydrophobic drugs. Liu et al. demonstrated that PEG-NH_2-functionalised GO nanoparticles (NGO-PEG) effectively delivered paclitaxel, a hydrophobic drug, by enhancing its solubility and stability in aqueous environments. The PEG-NH_2 coating creates a hydrophilic barrier that prevents aggregation, while strong hydrophobic interactions between paclitaxel and the GO surface improve drug loading capacity. This dual functionality resulted in superior tumour inhibition compared to free paclitaxel [17]. These findings underscore the multifunctionality of PEG-NH_2, which not only improves interaction, stability and adaptability but also optimizes the efficacy of therapeutic applications by addressing critical challenges such as drug solubility and controlled release. This balance of stability and adaptability highlights the importance of designing hybrid systems with interaction types tailored to their application through a combination of experimental and computational approaches.

In addition to drug delivery, PEG-NH_2 also plays a crucial role in antimicrobial applications. For instance, Ag and Cu nanoparticles offer significant advantages over traditional antibacterial drugs due to their broad-spectrum activity and reduced bacterial resistance [30,31]. Studies have shown that incorporating PEG-NH_2 into GO enhances their effectiveness by facilitating the formation of stable covalent bonds with functionalised metal nanoparticles [32,33]. This functionalisation improves the binding affinity with metal nanoparticles and stability of the nanoparticles, effectively addressing common stability issues of nanoparticles such as aggregation and dissociation [34,35]. In antimicrobial applications, both covalent and non-chemical bindings play a crucial role in the performance of functionalised GO surfaces, such as GO-PEG-NH_2, with metal nanoparticles. Among the non-covalent interactions, at physiological pH, the functional groups on GO-PEG-NH_2 primarily rely on weaker Van der Waals forces due to the neutral state of PEG-NH_2. However, the surface charge of metal nanoparticles, which depends on their synthesis, can be tailored to optimise electrostatic interactions at this pH, improving the adhesion and stability of nanoparticles on functionalised GO surfaces and enhancing their antimicrobial efficacy. Additionally, at neutral pH, coordination interactions between the amino groups of PEG-NH_2 and metals with incomplete d orbitals, such as Ag or Cu, can also play a significant role. These non-covalent interactions further stabilise and immobilize metal nanoparticles, complementing electrostatic and Van der Waals forces. In microenvironments where local pH drops (e.g., near bacterial biofilms), the pH-responsive behaviour of PEG-NH_2 may further promote electrostatic interactions, providing an adaptive advantage for targeted antimicrobial activity. By leveraging the dual functionality of PEG-NH_2, these mechanisms collectively optimise the performance of antimicrobial systems [26,36,37]. A study by Bao et al. demonstrated the evidence that 8-arm PEG-functionalised GO-AgNPs showed improved dispersion stability with improved antibacterial performance in physiological solutions [37]. These results highlight the potential of PEGylation to optimise nanoparticle systems for advanced biomedical applications. Further exploration of diverse PEG-NH_2 architectures and their integration with GO could unlock additional benefits, enhancing the reliability, stability, and overall efficacy of these systems in critical antimicrobial and therapeutic contexts.

Materials Studio is a versatile platform for modelling and simulating material properties at the molecular level, supporting both classical and quantum mechanical methods [38,39]. The FORCITE module within Materials Studio excels in classical MD simulations, solving Newton's equations of motion to obtain structural, dynamic, and thermodynamic properties of systems [40,41]. While other tools like Gaussian and Vienna *ab* initio simulation package (VASP) are used for *ab* initio calculations, which solve the Schrödinger equation to obtain electronic properties, these methods are computationally intensive and suited for smaller systems [42,43]. In contrast, FORCITE's efficient COMPASSII force field allows it to handle larger systems and extended simulation times effectively, making it especially useful for examining interaction energies, binding affinities, and the impact of functional groups on nanoparticle behaviour [44,45,46].

While significant progress has been made in exploring the properties and applications of GO and its functionalised derivatives, much of the existing research remains limited in scope, often isolating the effects of GO functionalisation or metal nanoparticle interactions. Furthermore, many studies neglect the integration of both experimental and theoretical approaches, leading to a fragmented understanding of these systems [19,37,44]. This study presents a novel approach by combining cutting-edge experimental techniques with molecular dynamics (MD) simulations to offer a comprehensive, multi-dimensional analysis. Unlike prior works, we explicitly compare numerical predictions with practical characterisation data, including scanning electron microscopy (SEM), energy-dispersive X-ray spectroscopy (EDS), transmission electron microscopy (TEM), UV–visible spectroscopy, Fourier-transform infrared spectroscopy (FTIR), Raman spectroscopy, and thermogravimetric analysis (TGA). This integrated methodology provides a holistic view of

the structural, morphological, and suspension stability characteristics of PEGylated GO functionalised with Cu and Ag nanoclusters, addressing key gaps in the current literature and offering a deeper understanding of the synergy between GO and metal nanoparticles.

2. Material and methods

2.1. Computational theory

2.1.1. Molecular dynamics simulations

MD simulations were employed to explore the interactions between graphene-based materials and small Cu and Ag nanoclusters, with a specific focus on how PEG-NH_2 chains influence these interactions The simulations aimed to elucidate the molecular mechanisms governing these interactions. To achieve this, the FORCITE module of Materials Studio 9 was utilised [47]. The simulations were performed within the NVT ensemble, which maintains a constant number of particles, volume, and temperature, for a duration of 1000 ps. Temperature control was managed at 298 K using a Nosé–Hoover thermostat, known for its efficiency in maintaining temperature stability throughout the simulation [48,49]. Electrostatic and van der Waals interactions were computed using an atom-based summation method with a cut-off distance of 12.5 Å, ensuring a balance between computational efficiency and accuracy. The COMPASSII force field was employed for calculating interactions between atoms, parameterised to accurately predict various properties of organic and inorganic materials [50], including graphene and graphene-based materials [51,52]. This force field considers only non-covalent interactions between the nanoclusters and graphene derivatives in the calculations, including electrostatic interaction and van der Waals forces, and it does not account for the simulation of chemical bond formation.

2.1.2. Molecular models for nanoclusters on graphene sheets

The graphene sheet for all graphene-derived materials seen in Fig. 1, was set at 24 × 19 $Å^2$. GO_{30} was modelled with a chemical formula of $C_{200}H_{61}O_{63}$, resulting in an O content of 29.03 % by weight. This model incorporated hydroxyl (–OH), epoxide (−O-), and carboxyl (–COOH) on the surface and edges of the graphene sheet. The modelling of GO_{30}-PEG-NH_2 involves grafting four PEG-NH_2 chains, each with a degree of polymerization (n = 10), onto a single GO_{30} sheet, yielding the chemical formula$C_{289}H_{245}N_8O_{100}$.

The initial structures were prepared by placing 13-atom icosahedral metal nanoclusters, representing Cu and Ag, 12 Å away from the graphene-based materials within a 40 × 40 × 40 $Å^3$ periodic simulation cell. These clusters were then surrounded by 2375 water molecules to simulate a realistic setting for studying the interactions between the metallic clusters and the graphene-derived materials. With the configurations established in Fig. 2, the next step involved quantifying these interactions by calculating the interaction energies using **Equation (1)** [50]:

$$\Delta E = E_{GBM+cluster} - (E_{GBM} + E_{cluster}) \quad (1)$$

where $E_{GBM+cluster}$ represents the equilibrium potential energy of the system with the cluster, while E_{GBM} and $E_{cluster}$ are the energies of the isolated graphene-based materials and clusters, respectively. These energies were averaged over the last 300 ps of each simulation. The mean squared displacement (MSD) of clusters was determined using **Equation (2)**:

$$MSD = \frac{1}{N}\sum_{i=1}^{N}\langle(r_i(0) - r_i(t))^2\rangle \quad (2)$$

where $r_i(0)$ is the initial position, $r_i(t)$ is the position at time and N is the number of atoms in the cluster. MSD was calculated from the particle positions along its trajectory using a time step of 5 ps.

2.2. Experimental methodology

2.2.1. Synthesis

Materials

Graphene oxide with a 30 % degree of oxidation (GO_{30}) was acquired from NanoInnova Technologies. The compound of 4arm-PEG5K-NH_2 (PEG-NH_2) was sourced from Sigma-Aldrich. Rest of chemical agents such as N-(3-Dimethylaminopropyl)-N'-ethylcarbodiimide hydrochloride (EDC-HCl), N-Hydroxysuccinimide 1-Hydroxy-2,5-pyrrolidinedione (NHS) and $AgNO_3$ and Trisodium citrate dihydrate ($Na_3C_6H_5O_7$) were also provided by Sigma-Aldrich. All materials were used as received unless otherwise indicated. Copper nanoparticles were sourced from CF Nanotechnology® (Suzhou, China) and ultra-pure deionized/distilled water was obtained using a lab-based Milli-Q system.

Synthesis of GO_{30}-PEG-NH_2

The synthesis procedure builds upon author's previous studies [53], with a minor modification of incorporating a combination of EDC-HCl and NHS into the system of PEGylation of GO_{30} as shown in Fig. 3.

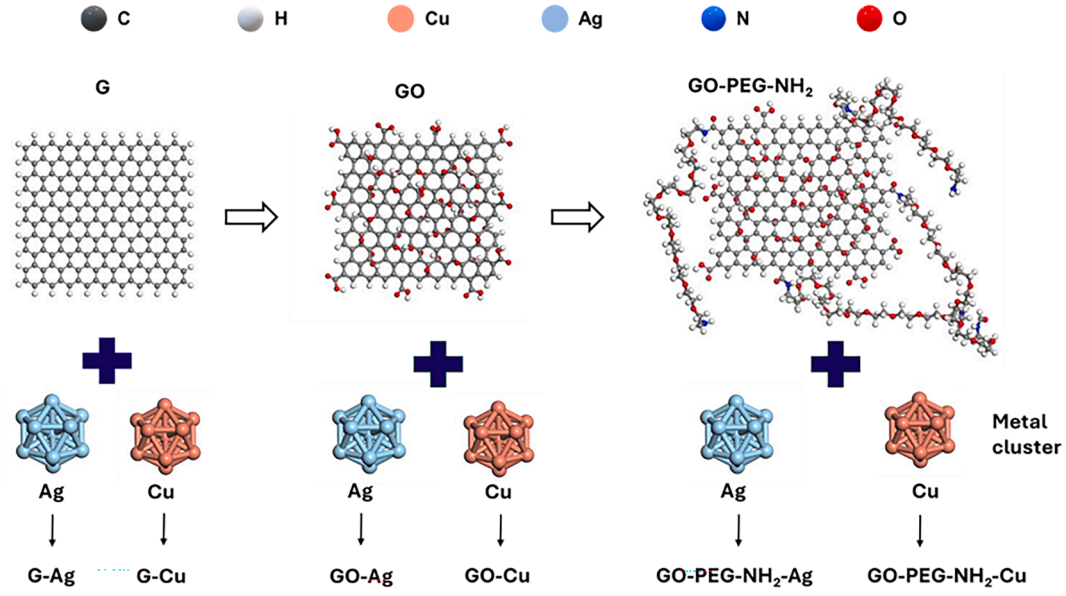

Fig. 1. Molecular models for studying metal cluster interactions with graphene-based materials.

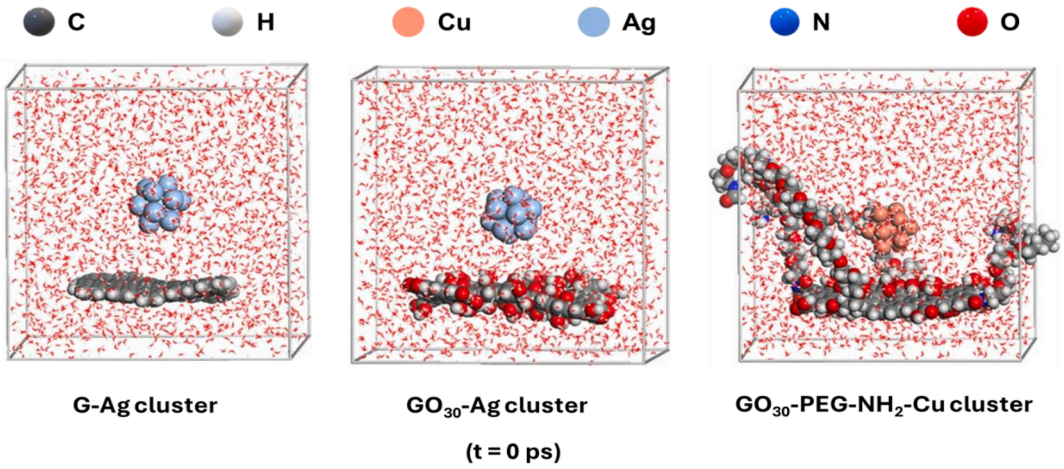

Fig. 2. Models for illustrating metallic nanocluster interactions with graphene, GO_{30}, and GO_{30}-PEG-NH_2 in hydrated conditions, shedding light on early alignment and distribution.

The combination of the pairing reagents effectively activates carboxyl groups, forming a stabilised intermediate that can significantly enhance the formation of an amide bond between the primary amine of PEG-NH_2 and the carboxyl group of GO_{30} [21].

In practice, the initial step in the synthesis involved dispersing 100 mg of GO_{30} in 100 ml of deionised water (1 mg/ml; 0.1 % w/v), followed by 20 min of ultrasonication to prevent agglomeration by disrupting the π-π interactions between graphene sheets. EDC-HCl and NHS were then introduced in a 1:1 M ratio, and the mixture was magnetically stirred at 60 rpm for 3 h. Subsequently, PEG-NH_2 was added, and followed by a second ultrasound dispersion cycle to enhance compound intercalation, subjected to magnetic stirring for 16 h. After PEGylation, the GO_{30}-PEG-NH_2 dispersions were purified through successive centrifugation cycles at 6000–6500 RCF, each lasting 30 min. The supernatant was removed after each cycle, and the precipitant was redissolved in deionized water to eliminate any unreacted materials and by-products. The resulting nanostructures were isolated through vacuum filtration using a vacuum pump, followed by drying in an oven at 40 °C for 2 h to ensure a thorough and expedited removal of residual moisture.

Synthesis of Ag nanoparticles

Ag nanoparticles were synthesized by chemical reduction using the Frens method [54,55], where $AgNO_3$ is used as a precursor and $Na_3C_6H_5O_7$ as a reducing and stabilising agent Fig. 4.

In a 50 mL of 1.0 mM $AgNO_3$ solution was placed, covered with Al foil and fitted with a magnetic stirrer. The solution was then heated under continuous stirring, and upon reaching its boiling point, 500 µL of 0.189 M $Na_3C_6H_5O_7$ was swiftly introduced. The mixture was stirred at 200 rpm for an additional 20 min while maintaining the boiling temperature. The Ag nanoparticles were then centrifuged at 2400 RCF for 30 min and resuspended in the desired volume of distilled water. Finally, the nanoparticles were stored at 4 °C in the dark, wrapped in Al foil.

Preparation of GO_{30}/GO_{30}-PEG-NH_2-Ag and GO_{30}/GO_{30}-PEG-NH_2-Cu suspensions

For the preparation of GO_{30} and GO_{30}-PEG-NH_2 suspensions with Ag and Cu nanoparticles, the materials (either in powdered or dispersed form) were mixed in a 30:70 wt ratio of GO_{30}/GO_{30}-PEG-NH_2 to Ag and Cu nanoparticles, maintaining a final nanocomposite concentration of 1 mg/ml in the suspension. The mixture was then sonicated in a liquid processor for 10 min at 50 % amplitude, using an applied pulse sequence of 20 s on and 5 s off, while being cooled in an ice bath. Following this, the dispersed suspensions were subjected to mechanical mixing for 16 h in a hybridization incubator at room temperature.

2.2.2. *Materials characterization*

Characterisation techniques focused on evaluating the size, distribution, and morphology of GO_{30}, GO_{30}-PEG and their conjugated with metal clusters. SEM imaging was performed at 20 kV using a JEOL JSM 6335F (JEOL Ltd., Tokyo, Japan) with a conductive carbon tape substrate, ensuring high-resolution imaging and accurate electron conduction. The SEM images were analysed to determine the probability distribution of metal clusters on the GO_{30} sheets, providing critical insights into the dispersion and uniformity of the nanocomposites.

TEM analysis, conducted with a JEM-2100 (JEM Ltd., Tokyo, Japan) operated at 200 kV, offered detailed imaging of the internal structure of the nanoparticles. For sample preparation, dispersions were diluted to 0.01 wt% and a drop was placed on a carbon-coated Cu grid.

UV–Visible spectroscopy was performed using a Thorlabs SLS205 fibre-coupled xenon light source, with the dispersed samples placed in a 10 mm path-length quartz cuvette. Absorption spectra were recorded across the UV to near-infrared (NIR) range, revealing the electronic structure and optical behaviour of the nanoparticles.

FT-IR spectroscopy was performed with a Nicolet iS50 FT-IR spectrometer (Thermo Scientific, Spain) equipped with a germanium ATR accessory (Miracle Single Reflection ATR, Pike, Spain) to identify functional groups, providing detailed insights into the chemical structure and confirming successful functionalisation. The powder samples were directly deposited onto the germanium crystal and secured with a compressor rod. Blank measurements were performed prior to each sample analysis. All spectra were recorded within the wavenumber range of 3700–700 cm^{-1}.

Raman spectroscopy was used to assess the structural and vibrational properties of PEGylated GO_{30} nanocomposites functionalised with Ag and Cu nanoclusters. A 532 nm DPSS laser was employed to enhance Raman signals. The setup included a 20x objective for beam positioning and photon collection, coupled with a HORIBA 1250 M spectrometer equipped with a 1200 gr/mm grating and 400 µm slit for high resolution. Samples were deposited on quartz slides, revealing structural modifications and strong Raman signal enhancement, indicative of successful functionalisation.

Additionally, thermal analysis (TGA) and derivative thermogravimetric analysis (DTA) of approximately 10 mg of the sample were carried out using Seiko SSC 5200 TG-DTA 320 System to determine the thermal stability by monitoring mass changes during heating in a helium atmosphere from 30 °C up to 1000 °C with a heating rate of 10 °C/min. Before heating, the sample was kept during 30 min with a flow rate of 100 mL/min of Helium to remove any air in the equipment.

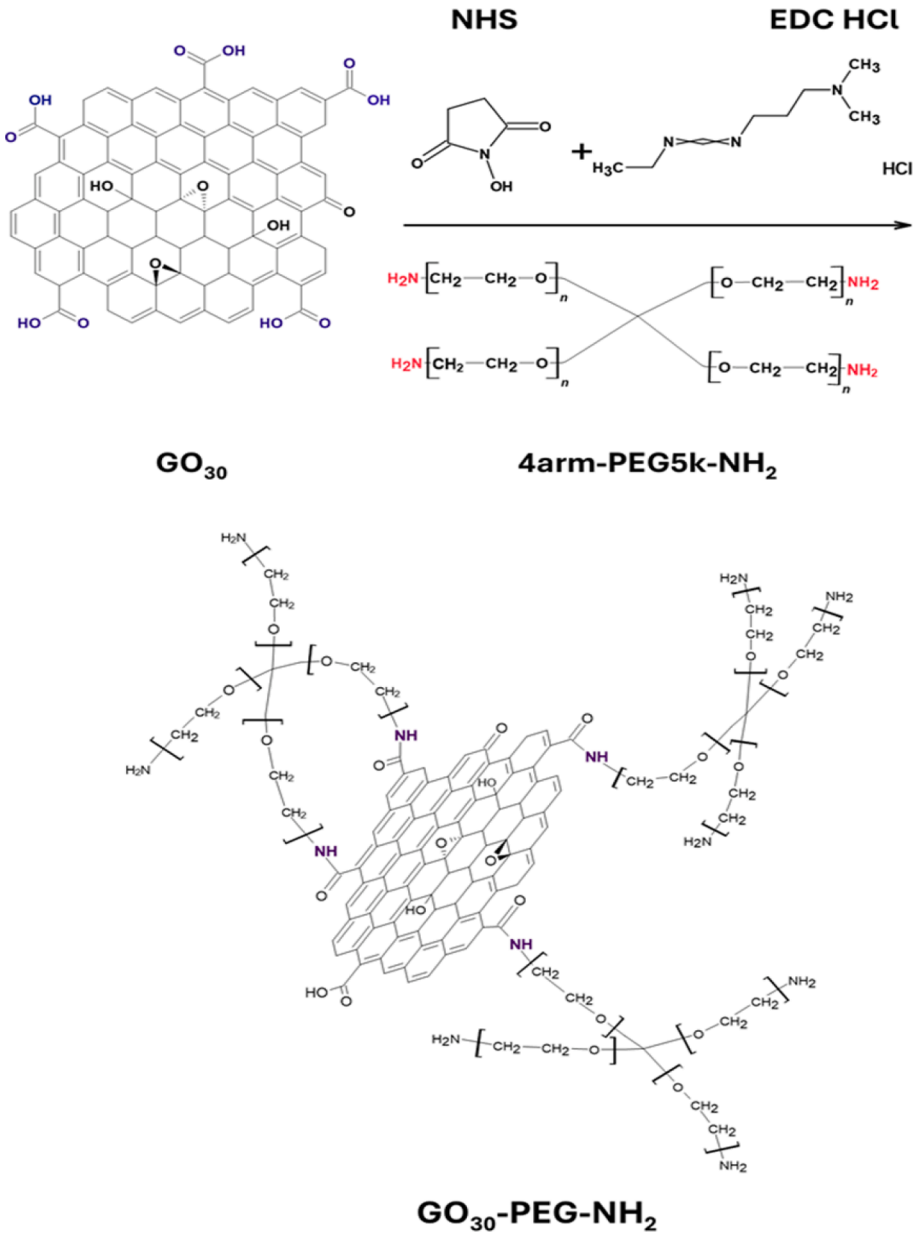

Fig. 3. A schematic illustration of chemical reaction pathway for the synthesis of GO_{30}-PEG-NH_2, is showcasing the PEGylation of GO_{30} via amide bond formation that facilitated by EDC-HCl and NHS activation of –COOH groups.

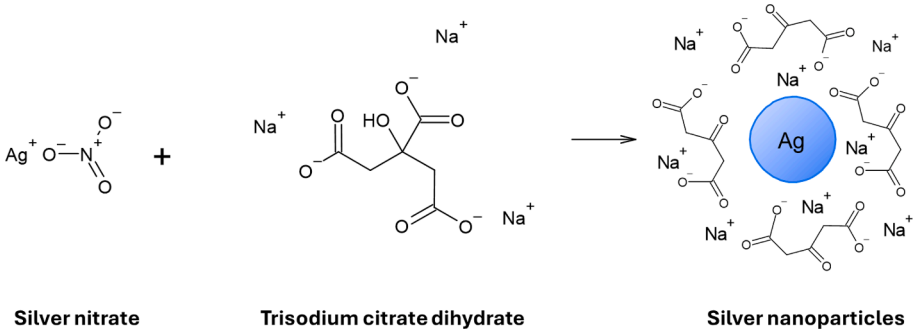

Fig. 4. Ag^+ ions were reduced to Ag nanoparticles using $Na_3C_6H_5O_7$ as the reducing agent. Byproducts such as citrate, oxalate, and acetone dicarboxylate are formed, affecting nanoparticle growth and stability.

3. Results and discussion

3.1. Molecular simulation

3.1.1. Interaction energies of metal clusters on functionalised graphene

The average interaction energy (ΔE) results, shown in Fig. 5 and calculated using **Eqn. (1)**, indicate that Ag clusters interact more strongly with graphene surfaces, including functionalised ones, GO_{30} and GO_{30}-PEG-NH_2, compared to Cu clusters. This is evidenced by the more negative ΔE values observed for Ag clusters in all cases [56,57]. For pristine graphene, Ag demonstrates a stronger interaction than Cu, with a ΔE difference of 29.18 kcal/mol. When graphene is oxidized to GO_{30}, ΔE for both metals become more negative, with Cu and Ag reaching values of −462.05 kcal/mol and −485.29 kcal/mol, respectively. Although the interaction energies increase in magnitude for both metals, the ΔE difference between GO_{30}-Ag and GO_{30}-Cu (23.24 kcal/mol) is slightly smaller than for pristine graphene, suggesting that oxidation enhances Cu's affinity through additional non-covalent interactions. However, Ag retains a stronger overall interaction [58].

PEGylation (GO_{30}-PEG-NH_2) further increases the interaction energy, with Cu reaching −497.91 kcal/mol and Ag −506.58 kcal/mol, representing an improvement of 35.86 kcal/mol for Cu and 21.29 kcal/mol for Ag compared to their oxidized form (GO_{30} only). PEGylation also reduces the ΔE difference between both metals to just 8.67 kcal/mol. This suggests that the PEG-NH_2 chains introduce stabilising forces, such as steric hindrance and non-covalent interactions, enhancing the affinity of both metals, with a stronger effect on Cu [59]. While Ag maintains stronger overall interaction energies, Cu shows a greater increase in affinity with GO and especially GO-PEG-NH_2, suggesting that graphene oxidation and PEGylation significantly enhance Cu adsorption compared to Ag. Further computational calculations and experimental validation with different configurations are needed to confirm this trend and assess Cu's capacity to generate more interactions.

3.1.2. Cluster stability on functionalised graphene sheets

The presence of PEG-NH_2 enhances these interactions by providing steric stabilisation, preventing cluster movement and aggregation through the formation of a physical barrier. This limits the proximity of clusters and reduces the likelihood of van der Waals-driven aggregation [19,34]. The final configurations of the systems, shown in Fig. 6, provide key insights into the interactions between metallic clusters and graphene-based sheets, consistent with similar studies involving graphene and metal nanoparticles [60,61]. Throughout the 1000 ps simulation, both Cu and Ag clusters remain firmly adhered to the graphene surfaces. Specifically, in the GO_{30}-PEG-NH_2-Ag system, Ag clusters interact closely with NH_2 groups located at the ends of the PEG chains on the GO_{30} sheets. Further calculations increasing the number of clusters would be needed to confirm this. A similar effect is observed for Cu in GO_{30}-PEG-NH_2, although Ag exhibits slightly stronger interaction energies. This aligns with findings reported by Y. K. Cheong et al., who demonstrated the effectiveness of Cu doped NH_2 functionalised GO as a catalyst for selective oxidation reactions [19]. Their work showed that functionalising GO with amines, such as those in PEG-NH_2, improves the distribution and stability of metal particles while enhancing the material's catalytic performance. GO-PEG-NH_2 serves as an excellent support for metallic nanoparticles by promoting dispersion, preventing agglomeration, and maximizing catalytic sites, reflecting the significant role of both PEG chains with –NH_2 groups in optimising interactions and functionality.

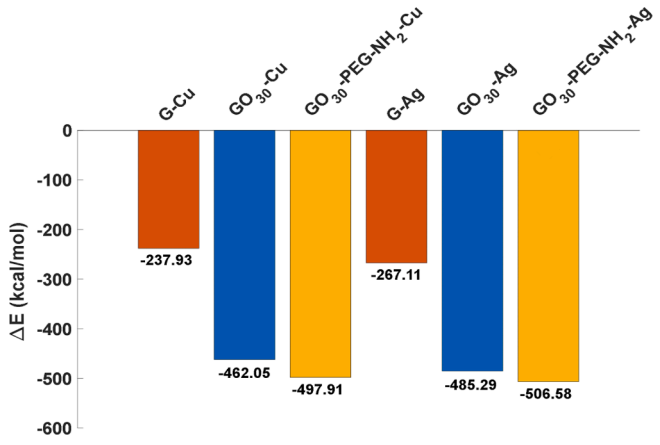

Fig. 5. The average interaction energy (ΔE) for Cu and Ag cluster adsorption on graphene and its functionalised forms indicates stronger interactions for Ag clusters. Surface functionalisation, particularly with PEGylated GO_{30} (GO_{30}-PEG-NH_2), further enhances these interactions.

3.1.3. Radial distribution function (RDF) analysis

The RDF analysis, shown in Fig. 7, reveals two main peaks within the short-distance range (up to ~ 6 Å), representing the most probable distances between the clusters and the surfaces. The first RDF peak indicates the closest adsorption distance and is directly correlated with the ΔE values. Pristine graphene (G) with Cu and Ag clusters shows the largest adsorption distances (~3.57 Å), indicating weaker interactions compared to the functionalised systems. Although the RDF peaks are more intense in these systems, suggesting a higher probability of finding clusters at a specific distance, the greater distance between the clusters and the surface significantly weakens non-covalent interactions. Graphene oxidation (GO_{30}) introduces functional groups on the surface that reduce the adsorption distance for both metals. In GO_{30}-Cu the first peak appears at 3.25 Å, while for GO_{30}-Ag is at 3.27 Å, reflecting stronger interactions than in G. These results suggest that the functional groups of GO_{30} improve interactions, promoting closer adsorption of the metal clusters to the surface. On the other hand, GO_{30}-PEG-NH_2 systems present the shortest adsorption distances for both metals, with values of 2.83 Å for both Cu and Ag. This shorter distance suggests stronger interactions, confirmed by the more negative interaction energies in these systems. PEGylation introduces additional interactions (steric hindrance and non-covalent interactions), which promote the proximity of the clusters to the surface and a more efficient adsorption dynamic, resulting in greater system stability, consistent with findings by I. Lado-Touriño and A. Páez-Pavón on nanoparticle dispersion in polymer nanocomposites [44].

The RDF profiles reflect only non-covalent interactions between clusters and graphene surfaces. Quantum mechanical calculations are needed to fully understand interaction mechanisms, including potential charge transfer involving metal d-orbitals, which cannot be captured by classical force fields like COMPASSII [62]. While charge transfer can occur, it is typically weak compared to the dominant van der Waals interactions governing metal-graphene systems [63,64].

3.1.4. Time-dependent adsorption and mobility of pegylated nanoclusters

PEGylation's impact on the adsorption dynamics of Cu and Ag nanoclusters on graphene-derived surfaces is clearly demonstrated in Fig. 8, revealing important trends in stability and interaction behaviour. PEGylation significantly enhances the stability of metal clusters, particularly in Cu-based systems, which initially display notable instability due to weaker initial interactions. In contrast, Ag-based systems exhibit more rapid and stable adsorption profiles, with minimal fluctuations after 200 ps, indicating inherently stronger interactions with both pristine and oxidized graphene. Notably, PEGylated systems, such as GO_{30}-PEG-NH_2-Cu, achieve stabilisation more quickly and with reduced fluctuations, highlighting PEG-NH_2's role in reducing surface mobility and promoting a more uniform adsorption profile.

The analysis of Cu and Ag nanoclusters' mobility in Fig. 9, as determined using **Eqn. (2)**, reveals that PEGylated systems like GO_{30}-PEG-NH_2-Cu and GO_{30}-PEG-NH_2-Ag exhibit significantly lower mean

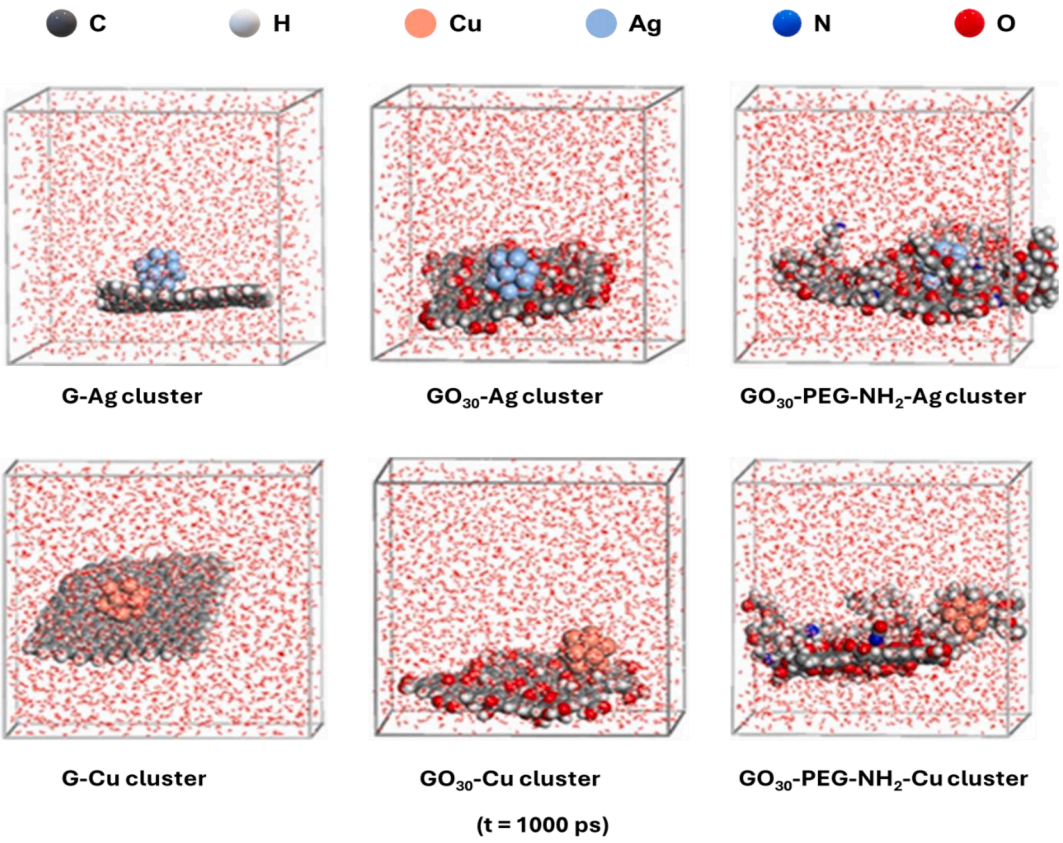

Fig. 6. Final positions of Cu and Ag clusters on graphene and functionalised GO_{30} sheets after 1000 ps of simulation. The clusters adhere closely to the surface, with PEG chains interacting and stabilising the nanoparticles, preventing their movement and aggregation.

squared displacement (MSD) values, around 20–30 $Å^2$ at 500 ps, indicating reduced cluster mobility due to stronger non-covalent interactions with the graphene surface. This reduced mobility corresponds with the increased stability seen in Fig. 8, where PEGylation led to more stable adsorption. Conversely, non-functionalised systems such as G-Cu and G-Ag show higher MSD values of approximately 150 $Å^2$ and 175 $Å^2$, respectively, reflecting weaker non-covalent interactions and greater mobility. PEGylation appears to effectively immobilize the clusters, likely due to steric hindrance from the PEG-NH_2 chains, which physically prevent cluster movement, and increased interaction strength with the graphene surface. This steric effect, combined with non-covalent interactions provided by PEG-NH_2, contributes to the observed stabilisation and reduced mobility of the nanoclusters.

These results suggest that PEGylation is crucial for optimising the stability and mobility of metal nanoclusters, which can significantly enhance the performance of nanocarriers in targeted drug delivery, improve sensing capabilities, and boost antimicrobial efficacy. The alignment between enhanced stability and reduced mobility underscores the potential of PEGylated nanoclusters for diverse applications. Further exploration through detailed experimental analyses will offer deeper insights into these materials' practical applications and their effectiveness in these fields.

3.2. Experimental results

3.2.1. SEM and EDS analysis

The SEM analysis in Fig. 10 highlights the deposition patterns of Ag and Cu nanoparticles on PEGylated and non-PEGylated GO_{30} sheets. In non-PEGylated samples (GO_{30}-Ag, GO_{30}-Cu), nanoparticles are sparsely distributed with uneven surface coverage, likely caused by weak van der Waals forces and insufficient steric hindrance [65]. This limited interaction reduces their stability and uniformity. In contrast, PEGylated samples (GO_{30}-PEG-NH_2-Ag, GO_{30}-PEG-NH_2-Cu) display significantly improved nanoparticle distribution, stronger surface interactions, and enhanced coverage due to PEG's steric and electrostatic stabilisation effects.

The EDS results corroborate these observations. For GO_{30}-Cu, Cu content is 28.6 %, indicating moderate nanoparticle retention, while GO_{30}-PEG-NH_2-Cu shows reduced Cu (13.9 %) and increased carbon (68.5 %), signifying the contribution of the PEG layer to improved dispersion and stability. Similarly, GO_{30}-Ag has low Ag content (4.1 %), reflecting uneven nanoparticle attachment, whereas GO_{30}-PEG-NH_2-Ag exhibits a higher Ag concentration (8.4 %) and elevated carbon (79.4 %), confirming PEGylation's role in enhancing surface interaction and retention. Trace Na and Cl peaks in PEGylated samples likely arise from residual ions during synthesis. Collectively, the results demonstrate that PEGylation significantly improves nanoparticle adhesion, dispersion, and stability, making the composites more suitable for applications such as antimicrobial systems, drug delivery, and energy storage.

3.2.2. Pegylation effects on nanoparticle size

The size distribution analysis in Fig. 11 highlights the impact of PEGylation on the size and uniformity of Cu and Ag nanoparticles attached to GO_{30} sheets, with a specific focus on the 10 to 100 nm range. This size range is crucial for optimising material properties and plasmonic activity, as nanoparticles within this range are large enough to avoid quantum size effects, ensuring sufficient electron density for effective collective oscillations. Additionally, they are small enough to avoid significant radiative damping, which can occur in larger particles and reduce plasmonic efficiency. The analysis shows that PEGylation significantly narrows the size distribution and reduces the average size of both Cu and Ag nanoparticles, concentrating most particles in the 10–20 nm range. For non-PEGylated samples, the distribution is broader, with fewer particles in the optimal size range, particularly for

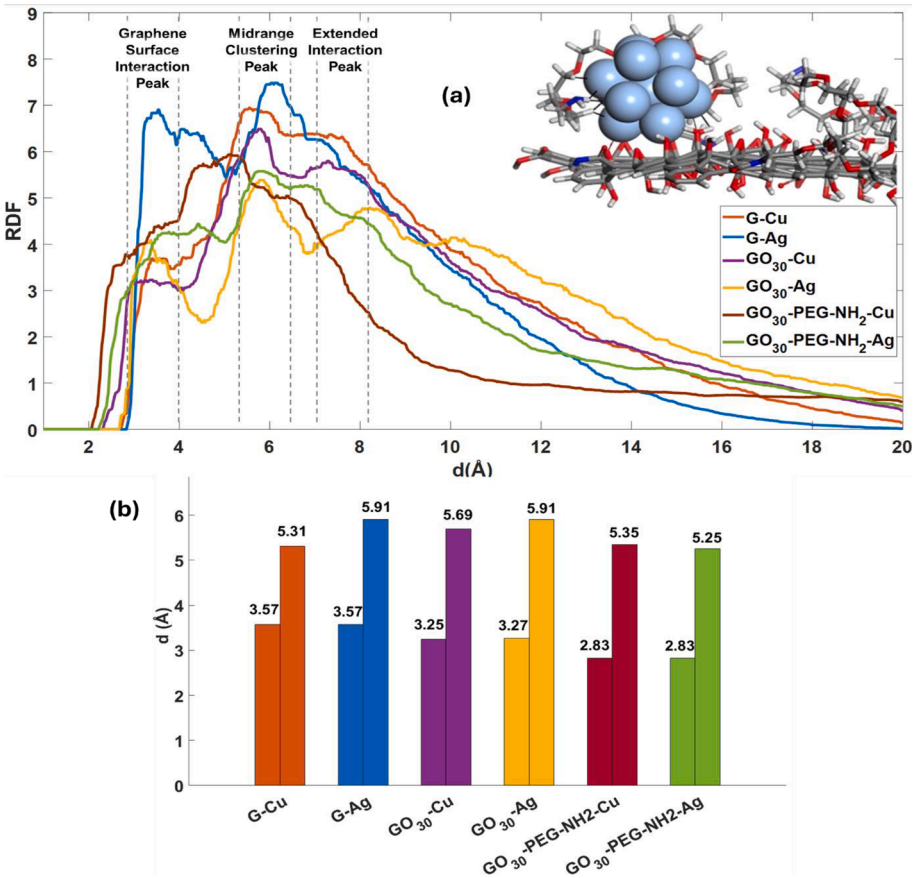

Fig. 7. (a) RDF analysis of Cu and Ag clusters with graphene, GO_{30}, and GO_{30}-PEG-NH_2, showing three interaction peaks. Inset: close contact (2.83 Å) between Ag clusters and GO_3-PEG-NH_2. (b) Bar graph of the first two RDF peaks for Cu and Ag clusters, indicating surface interactions and midrange clustering.

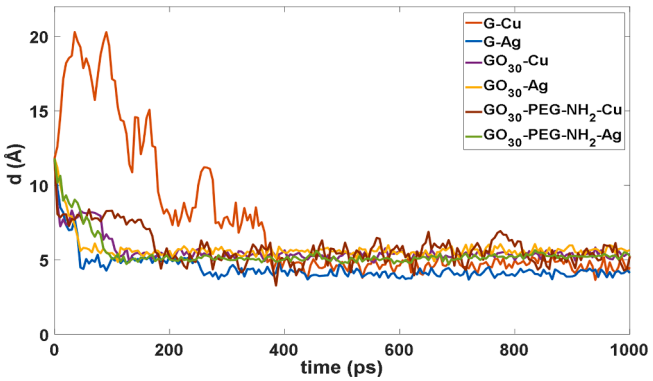

Fig. 8. Time-dependent variation in the distance between the cluster's centre of mass and the surface of the graphene-derived material.

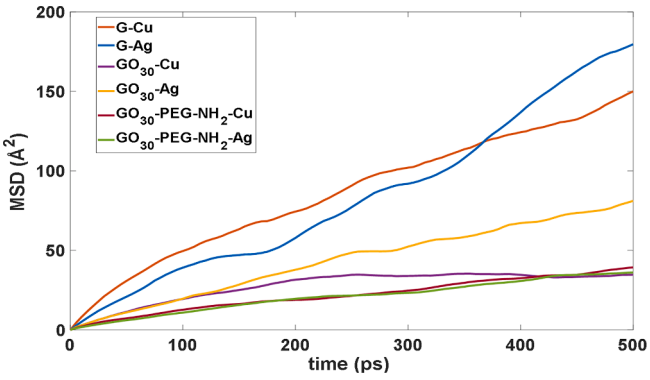

Fig. 9. MSD of Cu and Ag nanoclusters over 500 ps, demonstrating reduced mobility in PEGylated systems compared to non-functionalised ones.

Cu, where the distribution extends across a wider range of diameters. This size control enhances the nanoparticles' antimicrobial and sensing properties, as smaller, uniformly distributed particles provide increased surface area for interactions and more consistent performance in applications such as pathogen detection and inactivation [66].

3.2.3. *TEM imaging*

The TEM analysis of GO_{30} composites with Cu and Ag nanoparticles, with and without PEG modification in Fig. 12, reveals key differences in internal structure and crystallography. In GO_{30}-Cu, significant nanoparticle aggregation and poor crystallographic alignment are observed, attributed to high surface energy and Ostwald ripening, leading to uneven dispersion [67,68]. The GO_{30}-PEG-NH_2-Cu sample shows improved dispersion and more uniform internal structures due to PEG's steric stabilisation, which mitigates aggregation. Similarly, GO_{30}-Ag displays better dispersion and structural consistency than Cu, benefiting from Ag's lower surface energy and stronger interactions with GO's oxygen-containing groups [69]. The PEGylated GO_{30}-Ag samples also exhibit improved dispersion and enhanced crystallographic order. These TEM observations are consistent with the size distribution analysis, shown in Fig. 11, which highlights how PEGylation effectively narrows the particle size range and maintains optimal sizes for improved material properties.

3.2.4. *UV–visible spectroscopy*

The UV–Vis spectrum in Fig. 13 reveals distinct properties between

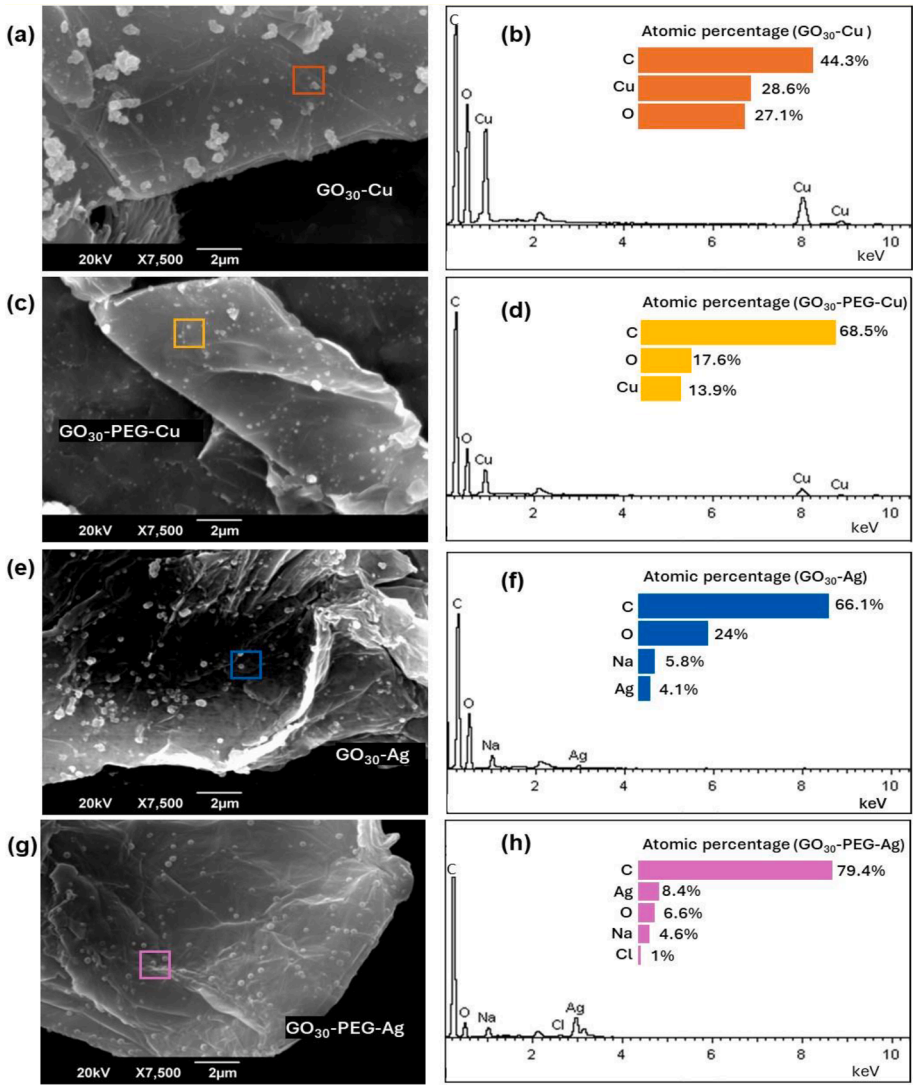

Fig. 10. SEM and EDS analysis of GO_{30} nanocomposites with Cu and Ag nanoparticles, with and without PEGylation. (a, b) GO_{30}-Cu shows uneven nanoparticle distribution with 28.6% Cu. (c, d) GO_{30}-PEG-NH_2-Cu demonstrates improved dispersion and reduced Cu content (13.9%). (e, f) GO_{30}-Ag exhibits sparse Ag clusters with 4.1% Ag. (g, h) GO_{30}-PEG-NH_2-Ag achieves better coverage and higher Ag content (8.4%).

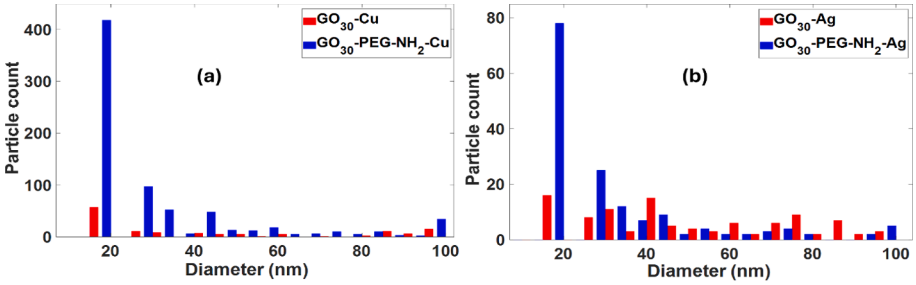

Fig. 11. Size distribution analysis of Cu (a) and Ag (b) nanoparticles on GO_{30} sheets, highlighting the impact of PEG functionalisation on particle size and stability, based on SEM analysis.

PEGylated and non-PEGylated Cu and Ag nanoparticles. Non-PEGylated Cu nanoparticles exhibit a peak around 225–232 nm, associated with $Cu2^+$ ions, undergoes a redshift to 260 nm in PEG-containing samples. This shift suggests changes in the electronic environment due to PEG's influence. PEG also enhances the peak at 290–300 nm associate with graphene π-π* transitions in both Cu and Ag nanoparticles, and reduces the shoulder around 300 nm, indicating decreased GO_{30} layer thickness [20]. PEGylated Cu samples show a broad peak around 600–700 nm, confirming Cu nanoparticles and their improved plasmonic response. For Ag nanoparticles, the surface plasmon resonance peak redshifts from 430 nm in bare Ag to 418 nm when conjugated with GO. However, upon PEGylation, the absorbance increases, maintaining consistent optical characteristics despite the interaction with graphene [37]. This suggests potential applications in fields like optical sensing and imaging, where

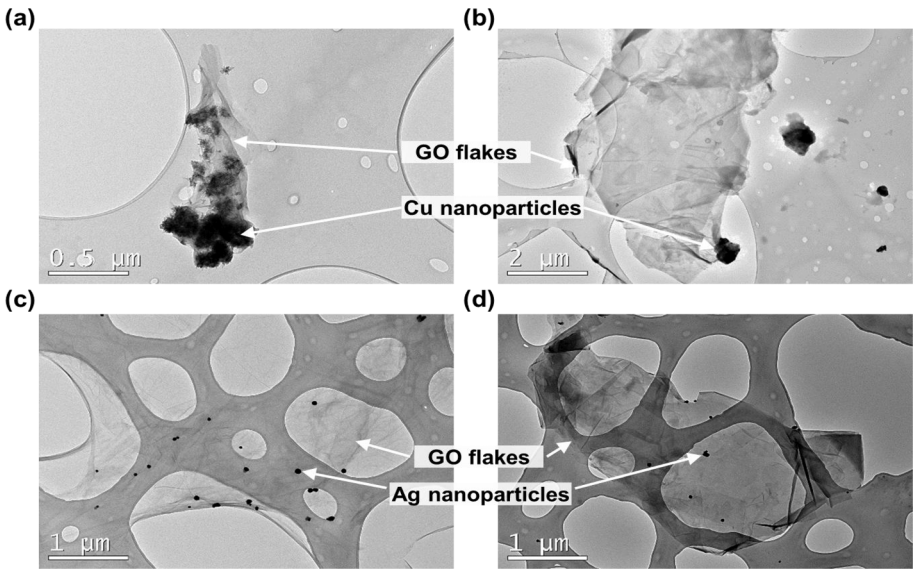

Fig. 12. TEM images of GO_{30} composites with Cu and Ag nanoparticles: (a) GO_{30}-Cu, (b) GO_{30}-PEG-NH_2-Cu (c) GO_{30}-Ag, and (d) GO_{30}-PEG-NH_2-Ag. PEG improves dispersion and stability, with GO_{30}-PEG –NH_2-Ag showing the most uniform nanoparticle distribution.

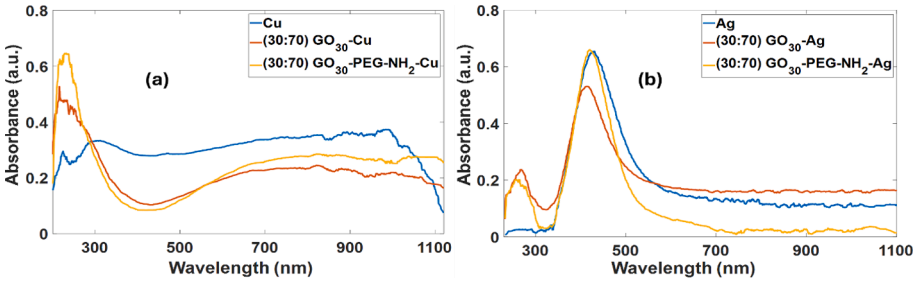

Fig. 13. UV–Visible spectra of GO_{30}-metal composites (30:70 ratio). (a) PEGylated GO_{30}-Cu displays a defined Cu^{2+} peak at 260 nm and a broad 600–700 nm peak. (b) GO_{30}-Ag with PEG exhibits a stabilised plasmon peak at 400–450 nm. Highlighting PEG's role in enhancing and stabilising optical features.

consistent and stable plasmonic responses are crucial for accurate signal detection and enhanced performance [70].

3.2.5. *Fourier transform infrared spectroscopy (FTIR)*

The FTIR spectrum in Fig. 14 confirms successful PEGylation and suggests physical interactions between Ag and Cu nanoparticles and GO_{30}/GO_{30}-PEG-NH_2. The GO_{30} spectrum displayed distinct bands characteristic of oxygen-containing groups, including a broad band at 3200–3600 cm^{-1} corresponding to the stretching of the O–H bond in –OH groups, both from surface hydroxyls and adsorbed water, and a band at 1726 cm^{-1} linked to C=O stretching in –COOH groups. Additionally, the band at 1618 cm^{-1} was associated with C=C stretching, indicating non-oxidised graphene regions, and the band around 1170 cm^{-1} corresponds to the antisymmetric stretching vibration of the C-O-C bond in the epoxy ring, while the peak at 1047 cm^{-1} is associated with the C-O stretching in the C-OH group [71].

These functional groups are indicative of the oxidation level of GO_{30} and contribute to its hydrophilicity and potential for further

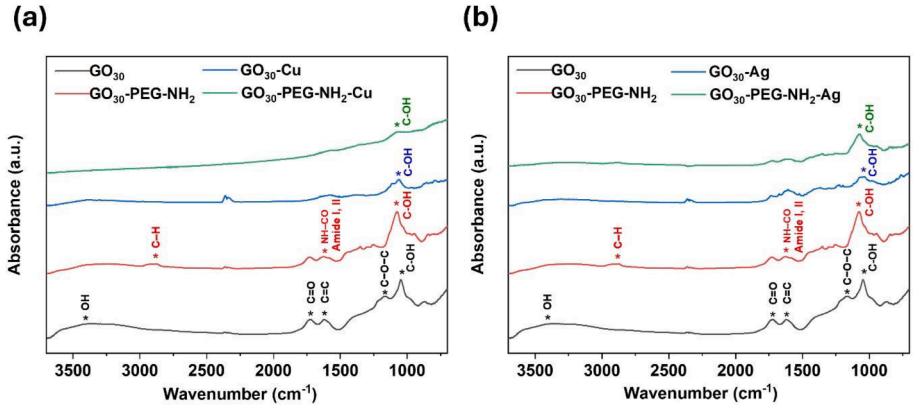

Fig. 14. FTIR spectra showing successful PEGylation of GO_{30}, with key changes in functional groups and subtle interactions with Ag and Cu nanoparticles, highlighting the modifications to the material's chemical structure.

functionalisation. Upon comparing the spectrum of GO_{30} with that of GO_{30}-PEG-NH_2 the emergence and modification of specific bands were observed. The band at 1623 $cm^{-}1$ corresponds to C=O stretching in the amide structure (Amide I band). Additionally, a 'shoulder' around 1580 $cm^{-}1$ suggests a secondary contribution from the Amide II band, associated with N–H bending. This overlap results in the asymmetry observed in the Amide I band, highlighting the presence of both vibrational modes [72]. A new peak appeared at approximately 2879 cm^{-1}, which was attributed to the stretching of C–H bonds in the $–CH_2$ groups of the PEG-NH_2 chains [19], and the peak at 1074 cm^{-1} likely results from a combination of C-O-C stretching in the ether groups of PEG-NH_2 and C-O stretching in the C-OH groups present in GO_{30}, as indicated by the band shift and the difference in the chemical environment [72].

While the FTIR spectra did not exhibit distinctive bands for the interaction between GO_{30}/GO_{30}-PEG-NH_2 and the Ag and Cu nanoparticles due to the nature of the interactions involved, subtle shifts and changes in band intensities suggested physical interactions, such as Van der Waals forces, electrostatic forces, and hydrogen bonding, between the metal clusters and the functional groups of the nanocomposites. The nature of these interactions directly influences the material's stability and performance [26].

3.2.6. Raman spectroscopy

The Raman spectrum of PEGylated GO_{30} nanocomposites with Ag and Cu nanoclusters seen in Fig. 15, highlights the structural and functional impacts of PEGylation. The D-band (1350 cm^{-1}) and G-band (1580 cm^{-1}) reflect the defect density and graphitic (sp^2) domains of GO_{30}, respectively. PEGylation enhances the uniformity of nanocluster distribution, which not only mitigates aggregation but also facilitates improved interactions with the GO surface. This effect is evident in the higher Raman signal intensities and elevated baselines observed for GO_{30}-PEG-NH_2-Ag and GO_{30}-PEG-NH_2-Cu. The elevated baseline further suggests that PEG chains increase the effective surface area and induce defect-related electronic states, amplifying the overall Raman response [19]. The higher I(D)/I(G) ratio in PEGylated samples, indicates an increase in defects or functional groups. While the rise in defect-related features may indicate a loss in structural integrity, it also enhances chemical reactivity and creates active sites for further functionalisation and reactions.

3.2.7. Thermal analysis

The TGA and DTG analysis in Fig. 16 reveals notable differences in the thermal stability of GO_{30} composites functionalised with PEG and metal nanoparticles. The initial mass loss around 120 °C, primarily due to the evaporation of adsorbed and interlayer water, is substantial for GO_{30} at 12.5 %, while GO_{30}-Cu and GO_{30}-Ag show significantly lower losses of 1.62 % and 1.7 %, respectively, indicating better water retention when functionalised with metal nanoparticles [73]. PEGylation increases this loss slightly, with GO_{30}-PEG-NH_2-Cu at 2.3 % and GO_{30}-PEG-NH_2-Ag at 1.8 %.

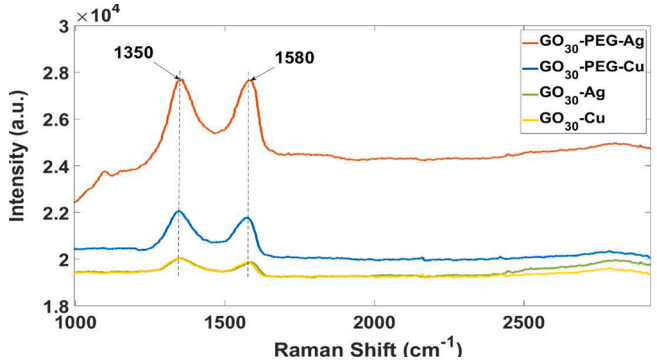

Fig. 15. Raman spectra of PEGylated GO_{30} nanocomposites with Ag and Cu nanoclusters, showing enhanced signal intensity and higher ID/IG ratio, indicating improved nanoparticle dispersion and increased defects for better reactivity.

In the critical decomposition range between 150 °C and 350 °C, where oxygen-containing functional groups decompose [74], GO_{30} exhibits a mass loss of 31.71 %, reflecting the instability of these functional groups. GO_{30}-Cu shows improved stability with a lower mass loss of 12.77 %, while GO_{30}-PEG-NH_2-Cu experiences a slightly higher loss of 18.59 %, suggesting that PEGylation introduces additional labile functional groups, thereby reducing thermal stability. Conversely, GO_{30}-Ag demonstrates greater stability with a mass loss of only 6.43 %, and GO_{30}-PEG-NH_2-Ag, despite PEGylation, maintains a relatively low loss of 10.35 %.

Notably, PEGylation broadens the decomposition peak around 120 °C, reflecting a more gradual and varied release of adsorbed water. Additionally, samples conjugated with metal nanoparticles display broader decomposition peaks beyond 200 °C compared to bare GO_{30}. This broadening suggests that the presence of metal nanoparticles affects the uniformity of thermal degradation and heat distribution, due to variations in interaction with the GO_{30} matrix and the distribution of metal particles within the composite. These multifunctional properties make PEGylated GO_{30} composites with metal nanoparticles promising for biomedical applications like targeted drug delivery and imaging, as well as for energy storage systems due to their enhanced stability and uniformity.

4. Conclusion

This study explores the interactions of graphene-based materials with small Cu and Ag nanoclusters, particularly focusing on the role of PEG-NH_2 chains. Key findings include:

1. **Interaction energies:** The interaction energies for both metals increase when graphene is oxidized to GO_{30}, with a greater improvement for Cu than Ag. The functionalisation of GO_{30} with PEG-NH_2 further enhances the affinity of both metals, particularly for Cu. While Ag continues to exhibit stronger interactions, the energy difference narrows with oxidation (23.24 kcal/mol) and PEGylation (8.67 kcal/mol), suggesting that Cu benefits more from these processes. Further computational analyses are necessary to better determine Cu's potential for forming additional interactions.
2. **Cluster stability and mobility:** The analysis of the mobility of Cu and Ag nanoclusters in PEGylated systems (GO_{30}-PEG-NH_2) reveals significantly lower mean squared displacement (MSD) values compared to non-functionalised systems, such as G-Cu and G-Ag, with ranges of 20–30 $Å^2$ and 150–175 $Å^2$ at 500 ps, respectively. This indicates reduced mobility, likely driven by steric stabilisation and enhanced non-covalent interactions.
3. **Nanoparticle distribution:** SEM and TEM analyses show that PEGylation leads to better dispersion and reduced aggregation of nanoparticles on GO_{30} sheets, narrowing the size distribution to 10–20 nm enhancing their effectiveness in sensing antimicrobial activity.
4. **Optical and thermal properties:** UV–Visible spectroscopy indicates PEGylated Ag nanoparticles exhibit a more stable plasmonic response at 400–450 nm. Metal nanoclusters significantly enhance thermal stability, with GO_{30}-Ag and GO_{30}-PEG-NH_2-Ag showing notably lower mass losses of 6.43 % and 10.35 %, respectively, while PEGylation broadens the decomposition peak around 120 °C, indicating improved heat distribution.

Overall, PEGylation significantly enhances the stability, dispersion, and functionality of metal nanoclusters on graphene-based materials, improving their potential for various applications in nanomedicine and material science.

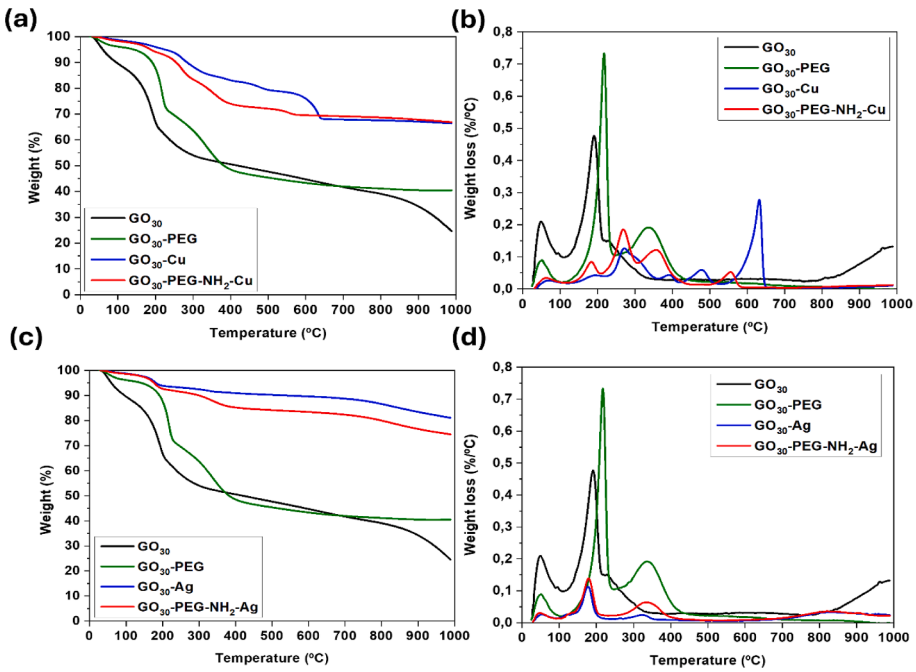

Fig. 16. TGA and DTG results reveal that GO_{30}-PEG-NH_2-Ag composites have superior thermal stability compared to GO_{30}-PEG-NH_2-Cu, making them better suited for high-temperature applications.

CRediT authorship contribution statement

Miriam Roldán-Matilla: Writing – review & editing, Writing – original draft, Methodology, Investigation, Formal analysis, Data curation. **Patrick Irigo:** Writing – review & editing, Writing – original draft, Visualization, Software, Formal analysis, Data curation. **María Luisa Rojas-Cervantes:** Writing – original draft, Methodology, Investigation, Data curation. **Mariana P. Arce:** . **Javier Pérez-Piñeiro:** Methodology, Data curation. **María Fuencisla Gilsanz:** Validation, Methodology, Formal analysis, Conceptualization. **Isabel Lado-Touriño:** Visualization, Validation, Investigation, Formal analysis, Data curation, Conceptualization. **Arisbel Cerpa-Naranjo:** Writing – review & editing, Visualization, Supervision, Conceptualization. **Guogang Ren:** .

Declaration of competing interest

The authors declare that they have no known competing financial interests or personal relationships that could have appeared to influence the work reported in this paper.

Acknowledgements

M.R.-M, M.P.A and A.C.-N thank the Fundación de la Universidad Europea for the Santander Bank Scholarship provided for the International Mobility of Professors and PhD Students, as well as the internal funds of the project (2022/UEM17). M.L.R-C thanks the Spanish Ministry of Science, Innovation and Universities (PID2021-126579OB-C32). The research project was also jointly initiated and partly funded by proof-of-concept funding from the University of Hertfordshire (UH-3500-RG-POC304).

Data availability

Data will be made available on request.

References

[1] S. Stankovich, D.A. Dikin, G.H.B. Dommett, K.M. Kohlhaas, E.J. Zimney, E.A. Stach, R.D. Piner, S.B. . Nguyen, R.S. Ruoff, Graphene-based composite materials, Nature 2006 442:7100, vol. 442, no. 7100, pp. 282–286, Jul. 2006, doi: 10.1038/nature04969.

[2] I.W. Frank, D.M. Tanenbaum, A.M. van der Zande, P.L. McEuen, Mechanical properties of suspended graphene sheets, J. Vacuum Sci. Technol. B: Microelectron. Nanometer Struct. Process. Measurement Phenomena 25 (6) (Nov. 2007) 2558–2561, https://doi.org/10.1116/1.2789446.

[3] F. Liu, M. Wang, Y. Chen, J. Gao, Thermal stability of graphene in inert atmosphere at high temperature, *J. Solid State Chem.* 276 (Aug. 2019) 100–103, https://doi.org/10.1016/J.JSSC.2019.04.008.

[4] K. Raidongia, A.T.L. Tan, J. Huang, Graphene oxide: some new insights into an old material, Carbon Nanotubes and Graphene: Edition 2 (Jan. 2014) 341–374, https://doi.org/10.1016/B978-0-08-098232-8.00014-0.

[5] Y. Zhu, S. Murali, W. Cai, X. Li, J.W. Suk, J.R. Potts, R.S. Ruoff, Graphene and graphene oxide: synthesis, properties, and applications, *Adv. Mater.* 22 (35) (Sep. 2010) 3906–3924, https://doi.org/10.1002/ADMA.201001068.

[6] T. Szabó, A. Szeri, I. Dékány, Composite graphitic nanolayers prepared by self-assembly between finely dispersed graphite oxide and a cationic polymer, *Carbon N Y* 43 (1) (Jan. 2005) 87–94, https://doi.org/10.1016/J.CARBON.2004.08.025.

[7] M. Hirata, T. Gotou, S. Horiuchi, M. Fujiwara, M. Ohba, Thin-film particles of graphite oxide 1: High-yield synthesis and flexibility of the particles, *Carbon N Y* 42 (14) (Jan. 2004) 2929–2937, https://doi.org/10.1016/J.CARBON.2004.07.003.

[8] Y.Y. Khine, X. Wen, X. Jin, T. Foller, R. Joshi, Functional groups in graphene oxide, *PCCP* 24 (43) (Nov. 2022) 26337–26355, https://doi.org/10.1039/D2CP04082D.

[9] R.K. Layek, A.K. Nandi, A review on synthesis and properties of polymer functionalised graphene, *Polymer (guildf)* 54 (19) (Aug. 2013) 5087–5103, https://doi.org/10.1016/J.POLYMER.2013.06.027.

[10] A. Pourjavadi, S. Asgari, S.H. Hosseini, Graphene oxide functionalised with oxygen-rich polymers as a pH-sensitive carrier for co-delivery of hydrophobic and hydrophilic drugs, *J Drug Deliv Sci Technol* 56 (Apr. 2020), https://doi.org/10.1016/J.JDDST.2020.101542.

[11] D.R. Dreyer, S. Park, C.W. Bielawski, R.S. Ruoff, The chemistry of graphene oxide, *Chem. Soc. Rev.* 39 (1) (Dec. 2009) 228–240, https://doi.org/10.1039/B917103G.

[12] K.P. Loh, Q. Bao, G. Eda, M. Chhowalla, Graphene oxide as a chemically tunable platform for optical applications, Nat. Chem. 2010 2:12, vol. 2, no. 12, pp. 1015–1024, Nov. 2010, doi: 10.1038/nchem.907.

[13] D. Bitounis, H. Ali-Boucetta, B. Hee Hong, D.-H. Min, K. Kostarelos, D. Bitounis, H. Ali-Boucetta, K. Kostarelos, B. Hee Hong, and D. Min, Prospects and Challenges of Graphene in Biomedical Applications, Adv. Mater. 25(16) (2013) 2258–2268, doi: 10.1002/ADMA.201203700.

[14] J. Wintterlin, M.L. Bocquet, Graphene on metal surfaces, *Surf. Sci.* 603 (10–12) (Jun. 2009) 1841–1852, https://doi.org/10.1016/J.SUSC.2008.08.037.

[15] V.C. Sanchez, A. Jachak, R.H. Hurt, A.B. Kane, Biological interactions of graphene-family nanomaterials: an interdisciplinary review, *Chem. Res. Toxicol.* 25 (1) (Jan. 2012) 15–34, https://doi.org/10.1021/TX200339H/ASSET/IMAGES/LARGE/TX-2011-00339H_0007.JPEG.

[16] K. Yang, J. Wang, B. Chen, Facile fabrication of stable monolayer and few-layer graphene nanosheets as superior sorbents for persistent aromatic pollutant management in water, *J Mater Chem A Mater* 2 (43) (Oct. 2014) 18219–18224, https://doi.org/10.1039/C4TA04300F.
[17] H. Xu, M. Fan, A.M.A. Elhissi, Z. Zhang, K.W. Wan, W. Ahmed, D.A. Phoenix, X. Sun, PEGylated graphene oxide for tumor-targeted delivery of paclitaxel, *Nanomedicine* 10 (8) (Apr. 2015) 1247–1262, https://doi.org/10.2217/NNM.14.233.
[18] T. Kamenska, M. Abrashev, M. Georgieva, N. Krasteva, Impact of polyethylene glycol functionalisation of graphene oxide on anticoagulation and haemolytic properties of human blood, *Materials* 14 (17) (2021) Sep, https://doi.org/10.3390/MA14174853.
[19] Y. K. Cheong, M. P. Arce, A. Benito, D. Chen, N. L. Crisóstomo, L. V. Kerai, G. Rodríguez, J. L. Valverde, M. Vadalia, A. Cerpa-Naranjo, et al., Synergistic antifunagal study of PEGylated graphene oxides and copper nanoparticles against Candida albicans, Nanomaterials 10 (2020) 819, doi: 10.3390/NANO10050819.
[20] A. Negi, K. Bijalwan, J. Rawat, H. Sharma, C. Dwivedi, Synthesis and characterization of the nanocomposites of graphene oxide in polyethylene glycol (PEG), *Mater. Today Proc.* 45 (Jan. 2021) 4742–4745, https://doi.org/10.1016/J.MATPR.2021.01.182.
[21] J. Charmi, H. Nosrati, J. Mostafavi Amjad, R. Mohammadkhani, H. Danafar, Polyethylene glycol (PEG) decorated graphene oxide nanosheets for controlled release curcumin delivery, Heliyon 5(4) (2019) e01466, doi: 10.1016/j.heliyon.2019.e01466.
[22] H. Samadian, R. Mohammad-Rezaei, R. Jahanban-Esfahlan, B. Massoumi, M. Abbasian, A. Jafarizad, M. Jaymand, A de novo theranostic nanomedicine composed of PEGylated graphene oxide and gold nanoparticles for cancer therapy, *J. Mater. Res.* 35 (4) (Feb. 2020) 430–441, https://doi.org/10.1557/jmr.2020.3.
[23] W. Zhuang, L. He, J. Zhu, J. Zheng, X. Liu, Y. Dong, J. Wu, J. Zhou, Y. Chen, H. Ying, Efficient nanobiocatalytic systems of nuclease P immobilized on PEG-NH2 modified graphene oxide: effects of interface property heterogeneity, *Colloids Surf. B Biointerfaces* 145 (Sep. 2016) 785–794, https://doi.org/10.1016/j.colsurfb.2016.05.074.
[24] K. Chauhan, J. Woo, W. Jung, D.-E. Kim, Poly(ethylene glycol)-engrafted graphene oxide for gene delivery and nucleic acid amplification, *Materials* 16 (23) (Nov. 2023) 7434, https://doi.org/10.3390/ma16237434.
[25] X. Pei, Z. Zhu, Z. Gan, J. Chen, X. Zhang, X. Cheng, Q. Wan, J. Wang, PEGylated nano-graphene oxide as a nanocarrier for delivering mixed anticancer drugs to improve anticancer activity, *Sci. Rep.* 10 (1) (Feb. 2020) 2717, https://doi.org/10.1038/s41598-020-59624-w.
[26] V. Georgakilas, J.N. Tiwari, K.C. Kemp, J.A. Perman, A.B. Bourlinos, K.S. Kim, R. Zboril, Noncovalent functionalisation of graphene and graphene oxide for energy materials, biosensing, catalytic, and biomedical applications, *Chem. Rev.* 116 (9) (May 2016) 5464–5519, https://doi.org/10.1021/acs.chemrev.5b00620.
[27] C. Liu, H. Li, J. Zhu, X. Huan, K. Xu, H. Geng, X. Guo, L. Ge, X. Jia, X. Yang, et al., Non-covalent and covalent-synergistical-interaction assembled GO self-supporting membrane with excellent alignment for ultrahigh H2 barrier applications, *Compos. B Eng.* 283 (Aug. 2024) 111652, https://doi.org/10.1016/j.compositesb.2024.111652.
[28] Y.-J. Park, S.Y. Park, I. In, Preparation of water soluble graphene using polyethylene glycol: comparison of covalent approach and noncovalent approach, *J. Ind. Eng. Chem.* 17 (2) (Mar. 2011) 298–303, https://doi.org/10.1016/j.jiec.2011.02.027.
[29] A. Jaggernauth, R.M. Silva, M.A. Neto, M.J. Hortigüela, G. Gonçalves, M.K. Singh, F.J. Oliveira, R.F. Silva, M. Vila, Nanographene oxide functionalisation with organic and hybrid organic–inorganic polymers by molecular layer deposition, *J. Phys. Chem. C* 120 (42) (Oct. 2016) 24176–24186, https://doi.org/10.1021/acs.jpcc.6b07909.
[30] D. Longano, N. Ditaranto, L. Sabbatini, L. Torsi, N. Cioffi, Synthesis and antimicrobial activity of copper nanomaterials, *Nano-Antimicrobials* 9783642244285 (Apr. 2014) 85, https://doi.org/10.1007/978-3-642-24428-5_3.
[31] T. Bruna, F. Maldonado-Bravo, P. Jara, N. Caro, Silver nanoparticles and their antibacterial applications, Int J Mol Sci, vol. 22, no. 13, Jul. 2021, doi: 10.3390/IJMS22137202.
[32] C. Luo, Y. Zhang, X. Zeng, Y. Zeng, Y. Wang, The role of poly(ethylene glycol) in the formation of silver nanoparticles, *J. Colloid Interface Sci.* 288 (2) (Aug. 2005) 444–448, https://doi.org/10.1016/J.JCIS.2005.03.005.
[33] T. Tang, Z. Liu, K. Wang, T. Wang, Y. Wang, Y. Ge, Copper nanoparticles supported on polyethylene glycol-modified magnetic Fe3O4 nanoparticles: Its anti-human gastric cancer investigation, *Arab. J. Chem.* 15 (1) (Jan. 2022) 103523, https://doi.org/10.1016/J.ARABJC.2021.103523.
[34] M. Xu, J. Liu, X. Xu, S. Liu, F. Peterka, Y. Ren, X. Zhu, Synthesis and comparative biological properties of Ag-PEG nanoparticles with tunable morphologies from Janus to multi-core shell structure, *Materials* 11 (10) (2018) Sep, https://doi.org/10.3390/MA11101787.
[35] R. Javed, M. Zia, S. Naz, S. O. Aisida, N. ul Ain, Q. Ao, Role of capping agents in the application of nanoparticles in biomedicine and environmental remediation: recent trends and future prospects, J. Nanobiotechnol. 18(1) (2020), doi: 10.1186/S12951-020-00704-4.
[36] K. Shankar, S. Agarwal, S. Mishra, P. Bhatnagar, S. Siddiqui, I. Abrar, A review on antimicrobial mechanism and applications of graphene-based materials, *Biomater. Adv.* 150 (Jul. 2023) 213440, https://doi.org/10.1016/j.bioadv.2023.213440.
[37] Y. Bao, H. Li, J. He, K. Song, H. Yu, C. Tian, J. Guo, X. Zhou, S. Liu, Polyethylene glycol modified graphene oxide-silver nanoparticles nanocomposite as a novel antibacterial material with high stability and activity, *Colloids Surf. B Biointerfaces* 229 (Sep. 2023) 113435, https://doi.org/10.1016/j.colsurfb.2023.113435.
[38] Y. Wang, H. Shao, C. Zhang, F. Liu, J. Zhao, S. Zhu, M.K.H. Leung, J. Hu, Molecular dynamics for electrocatalysis: mechanism explanation and performance prediction, *Energy Rev.* 2 (3) (Sep. 2023) 100028, https://doi.org/10.1016/J.ENREV.2023.100028.
[39] R. Li, J. Jiang, Y. Li, P. Ren, B. Shen, J. Qin, J. Zhang, M. An, P. Yang, Theoretical and experimental studies on the electrodeposited nanocrystalline Ag coatings from a novel Ag2O-based non-cyanide electrolyte, *J. Ind. Eng. Chem.* 131 (Mar. 2024) 432–440, https://doi.org/10.1016/J.JIEC.2023.10.046.
[40] Z. Wang, M. Su, X. Duan, X. Yao, X. Han, J. Song, L. Ma, Molecular dynamics simulation of the thermomechanical and tribological properties of graphene-reinforced natural rubber nanocomposites, *Polymers (Basel)* 14 (23) (2022) Dec, https://doi.org/10.3390/POLYM14235056.
[41] A. Fereidoon, S. Aleaghaee, I. Taraghi, Mechanical properties of hybrid graphene/TiO2 (rutile) nanocomposite: A molecular dynamics simulation, *Comput. Mater. Sci* 102 (May 2015) 220–227, https://doi.org/10.1016/J.COMMATSCI.2015.02.044.
[42] G. Sun, J. Kürti, P. Rajczy, M. Kertesz, J. Hafner, G. Kresse, Performance of the Vienna ab initio simulation package (VASP) in chemical applications, *J. Mol. Struct. (Thoechem)* 624 (1–3) (Apr. 2003) 37–45, https://doi.org/10.1016/S0166-1280(02)00733-9.
[43] L. Füsti-Molnár, P. Pulay, Gaussian-based first-principles calculations on large systems using the Fourier Transform Coulomb method, *J. Mol. Struct. (Thoechem)* 666–667 (Dec. 2003) 25–30, https://doi.org/10.1016/J.THEOCHEM.2003.08.114.
[44] I. Lado-Touriño, A. Páez-Pavón, Interaction between graphene-based materials and small ag, cu, and cuo clusters: A molecular dynamics study, *Nanomaterials* 11 (6) (Jun. 2021) 1378, https://doi.org/10.3390/NANO11061378/S1.
[45] M. Reil, J. Hoffman, P. Predecki, M. Kumosa, Graphene and graphene oxide energetic interactions with polymers through molecular dynamics simulations, *Comput. Mater. Sci* 211 (Aug. 2022) 111548, https://doi.org/10.1016/J.COMMATSCI.2022.111548.
[46] G. Nafie, G. Vitale, L. Carbognani Ortega, N. N. Nassar, Nanopyroxene grafting with β-cyclodextrin monomer for wastewater applications, ACS Appl Mater Interfaces, vol. 9, no. 48, pp. 42393–42407, Dec. 2017, doi: 10.1021/ACSAMI.7B13677.
[47] "BIOVIA Materials Studio | Dassault Systèmes." Accessed: Aug. 09, 2024. [Online]. Available: https://www.3ds.com/products/biovia/materials-studio.
[48] S. Nosé, A molecular dynamics method for simulations in the canonical ensemble, Mol. Phys. 52 (2) (1984) 255–268, https://doi.org/10.1080/00268978400101201.
[49] W.G. Hoover, Canonical dynamics: equilibrium phase-space distributions, *Phys Rev A (Coll Park)* 31 (3) (Mar. 1985) 1695, https://doi.org/10.1103/PhysRevA.31.1695.
[50] L. Piela, Ideas of Quantum Chemistry, Ideas of Quantum Chemistry, pp. 1–1086, Jan. 2007, doi: 10.1016/B978-0-444-52227-6.X5000-5.
[51] A. Einstein, A new determination of molecular dimensions, *Ann. Phys.* 324 (2) (Jan. 1906) 289–306, https://doi.org/10.1002/ANDP.19063240204.
[52] R. Metzler, J.H. Jeon, A.G. Cherstvy, E. Barkai, Anomalous diffusion models and their properties: non-stationarity, non-ergodicity, and ageing at the centenary of single particle tracking, *PCCP* 16 (44) (Oct. 2014) 24128–24164, https://doi.org/10.1039/C4CP03465A.
[53] J. Pérez-Piñeiro, F. Sánchez-Cea, M. P. Arce, I. Lado-Touriño, M. L. Rojas-Cervantes, M. F. Gilsanz, D. Gallach-Pérez, R. Blasco, N. Barrios-Bermúdez, and A. Cerpa-Naranjo, "Stability Study of Graphene Oxide-Bovine Serum Albumin Dispersions," J. Xenobiotics 13(1) (2023) 90-101, doi: 10.3390/JOX13010008.
[54] M. Gakiya-Teruya, L. Palomino-Marcelo, J.C.F. Rodriguez-Reyes, Synthesis of highly concentrated suspensions of silver nanoparticles by two versions of the chemical reduction method, Methods Protocols 2(1) (2019) 3, doi: 10.3390/MPS2010003.
[55] B. Pascu, A. Negrea, M. Ciopec, N. Duteanu, P. Negrea, L. A. Bumm, O. Grad, N.S. Nemeş, C. Mihalcea, D.M. Duda-Seiman, Silver nanoparticle synthesis via photochemical reduction with sodium citrate, Int. J. Mol. Sci. 2023 24(1) (2055) 255, doi: 10.3390/IJMS24010255.
[56] M. M. Mirhosseini, V. Haddadi-Asl, S.S. Zargarian, Fabrication and characterization of hydrophilic poly(ε-caprolactone)/pluronic P123 electrospun fibers, J. Appl. Polym. Sci. 133(17), doi: 10.1002/APP.43345.
[57] R.L. White, C.M. White, H. Turgut, A. Massoud, Z.R. Tian, Comparative studies on copper adsorption by graphene oxide and functionalised graphene oxide nanoparticles, *J. Taiwan Inst. Chem. Eng.* 85 (Apr. 2018) 18–28, https://doi.org/10.1016/J.JTICE.2018.01.036.
[58] W. Gao, L.B. Alemany, L. Ci, P.M. Ajayan, New insights into the structure and reduction of graphite oxide, Nat. Chem. 1(5) (2009) 403–408, doi: 10.1038/nchem.281.
[59] T. Gillich, C. Acikgöz, L. Isa, A.D. Schlüter, N.D. Spencer, M. Textor, PEG-stabilised core-shell nanoparticles: impact of linear versus dendritic polymer shell architecture on colloidal properties and the reversibility of temperature-induced aggregation, *ACS Nano* 7 (1) (Jan. 2013) 316–329, https://doi.org/10.1021/NN304045Q/SUPPL_FILE/NN304045Q_SI_001.PDF.
[60] M. Shukla, A. Verma, S. Kumar, S. Pal, I. Sinha, Experimental and DFT calculation study of interaction between silver nanoparticle and 1-butyl-3-methyl imidazolium tetrafluoroborate ionic liquid, Heliyon 7(1) (2021), doi: 10.1016/j.heliyon.2021.e06065.
[61] I. Lado-Touriño, A.C. Naranjo, M.P. Arce, A molecular dynamics modelling adsorption study of Cu and Ag nanoparticles on pristine and functionalised graphene surfaces, *Mater. Today Proc.* 33 (Jan. 2020) 1830–1834, https://doi.org/10.1016/J.MATPR.2020.05.065.

[62] C.R.C. Rêgo, P. Tereshchuk, L.N. Oliveira, J.L.F. Da Silva, Graphene-supported small transition-metal clusters: a density functional theory investigation within van der Waals corrections, *Phys. Rev. B* 95 (23) (Jun. 2017) 235422, https://doi.org/10.1103/PHYSREVB.95.235422/FIGURES/5/MEDIUM.

[63] R.M. Del Castillo, L.E. Sansores, Study of the electronic structure of Ag, Au, Pt and Pd clusters adsorption on graphene and their effect on conductivity, Eur. Phys. J. B 88(10) (2015) 1–13, doi: 10.1140/EPJB/E2015-60001-2.

[64] M. Berahman, M.H. Sheikhi, A. Zarifkar, H. Nadgaran, Structural and electronic properties of zigzag graphene nanoribbon decorated with copper cluster, *J. Comput. Electron.* 14 (1) (Mar. 2015) 270–279, https://doi.org/10.1007/S10825-014-0650-4/METRICS.

[65] S. Khorrami, Z. Abdollahi, G. Eshaghi, A. Khosravi, E. Bidram, A. Zarrabi, An improved method for fabrication of Ag-GO nanocomposite with controlled anti-cancer and anti-bacterial behavior; a comparative study, Scientific Reports 9(1) (2019) 1–10, doi: 10.1038/s41598-019-45332-7.

[66] J. Liu, C. Li, T. Brans, A. Harizaj, S. Van de Steene, T. De Beer, S. De Smedt, S. Szunerits, R. Boukherroub, R. Xiong, et al., Surface functionalisation with polyethylene glycol and polyethyleneimine improves the performance of graphene-based materials for safe and efficient intracellular delivery by laser-induced photoporation, *Int. J. Mol. Sci.* 21 (4) (Feb. 2020) 1540, https://doi.org/10.3390/IJMS21041540.

[67] S.T. Gentry, S.F. Kendra, M.W. Bezpalko, Ostwald ripening in metallic nanoparticles: stochastic kinetics, *J. Phys. Chem. C* 115 (26) (Jul. 2011) 12736–12741, https://doi.org/10.1021/JP2009786/SUPPL_FILE/JP2009786_SI_001.PDF.

[68] S. Shrestha, B. Wang, P. Dutta, Nanoparticle processing: understanding and controlling aggregation, *Adv. Colloid Interface Sci.* 279 (May 2020), https://doi.org/10.1016/J.CIS.2020.102162.

[69] K. Garg, P. Papponen, A. Johansson, N. Puttaraksa, L. Gilbert, Preparation of graphene nanocomposites from aqueous silver nitrate using graphene oxide's peroxidase-like and carbocatalytic properties, *Sci. Rep.* 10 (1) (2020) Dec, https://doi.org/10.1038/S41598-020-61929-9.

[70] Y. Zhu, M.D. Stoller, W. Cai, A. Velamakanni, R.D. Piner, D. Chen, R.S. Ruoff, Exfoliation of graphite oxide in propylene carbonate and thermal reduction of the resulting graphene oxide platelets, *ACS Nano* 4 (2) (Feb. 2010) 1227–1233, https://doi.org/10.1021/NN901689K/SUPPL_FILE/NN901689K_SI_001.PDF.

[71] R. Zhao, M. Lv, Y. Li, M. Sun, W. Kong, L. Wang, S. Song, C. Fan, L. Jia, S. Qiu, et al., Stable nanocomposite based on PEGylated and silver nanoparticles loaded graphene oxide for long-term antibacterial activity, *ACS Appl. Mater. Interfaces* 9 (18) (May 2017) 15328–15341, https://doi.org/10.1021/ACSAMI.7B03987/SUPPL_FILE/AM7B03987_SI_001.PDF.

[72] Z. Qi, J. Shi, Z. Zhang, Y. Cao, J. Li, S. Cao, PEGylated graphene oxide-capped gold nanorods/silica nanoparticles as multifunctional drug delivery platform with enhanced near-infrared responsiveness, *Mater. Sci. Eng. C* 104 (Nov. 2019) 109889, https://doi.org/10.1016/J.MSEC.2019.109889.

[73] C. Rodríguez-González, P. Velázquez-Villalba, P. Salas, V.M. Castaño, Green synthesis of nanosilver-decorated graphene oxide sheets, *IET Nanobiotechnol.* 10 (5) (Oct. 2016) 301, https://doi.org/10.1049/IET-NBT.2015.0043.

[74] Y. Yang, T. Liu, Fabrication and characterization of graphene oxide/zinc oxide nanorods hybrid, *Appl. Surf. Sci.* 257 (21) (Aug. 2011) 8950–8954, https://doi.org/10.1016/J.APSUSC.2011.05.070.